QIRT 10
http://dx.doi.org/10.21611/qirt.2010.145
10th International Conference on Quantitative InfraRed Thermography
July 27-30, 2010, Québec (Canada)

Some novel approaches to thermal tomography of CFRP composites

by V. Vavilov, D. Nesteruk, V. Shirayev, A. Ivanov

Tomsk Polytechnic University, Tomsk, Russia 634028, vavilov@introscopy.tpu.ru

Abstract

Thermal tomography is assumed to be a technique which allows sorting out hidden defects by their depths. In this paper, some novel approaches to the classification of defects by depths and material layers are discussed, namely no-reference dynamic tomography, defect characterization, neural networks and non-linear fitting.

1. Introduction

In this study, we use the definition of tomography borrowed from Internet (from Greek *τομη* — layer, or section) where tomography is regarded as a nondestructive technique (NDT) for layer-by-layer profiling of solids structure.

A bunch of tomographic techniques which implement analysis of temperature is being explored by several research teams worldwide (see Table 1).

Table 1. Thermal (infrared) tomography techniques

Technique	Description	Reference
Thermal-wave slice diffraction tomography	A particular implementation of the photothermal method (identification of thermal diffusivity distribution).	[1]
IR emission tomography of flames	The basic principle is identical to the 'classical' computer (X ray) tomography. Temperature distributions in gases and plasma are captured from few angles of view by using an IR imager.	[2]
Microwave tomography of human bodies	The technique uses semi-transparency of biological tissues to microwave radiation of wavelengths in a centimeter range.	[3,4]
IR tomography of excess charge carriers (in silicon)	The method was elaborated for the evaluation of life time and diffusion length of charge carriers in silicon samples by size up to 1 m. It is based on probing a tested object with crossed laser beams. A pumping laser (1.17-1.18 μm wavelength) injects electrons and holes, and a probing laser (3.39 μm) analyses spatial/temporal evolution of excess charge carriers. The accuracy of determining spatial coordinates is ~ 1 cm.	[5]
Acoustic thermo-tomography of biological objects	This passive technique enables the profiling of temperature through a human body. The identification procedure is based on solving the corresponding inverse (ill-posed) problem.	[6]
Stereoscopic two-sided tomography	A sample is heated with two sources and the temperature is monitored on the rear surface. Defect depth is determined by a simple geometrical equation.	[7]
Dynamic thermal tomography	In a one-sided thermal NDT (TNDT) procedure, deeper defects produce surface temperature signals at longer times. 'Timegrams' can be converted into 'tomograms', or 'depthgrams'	[8]
Thermal tomography based on the analysis of heat transfer function	Sample internal structure is identified by evaluating the heat transfer function.	[9]
Thermal tomography based on non-linear numerical fitting	Least-square multi-parametric fitting allows the evaluation of several parameters in a particular pixel, including defect depth and size. Producing a full-frame image requires too much of computer time.	[10, 11]
Defect characterization approach	Some inversion formulas have been proposed to evaluate defect depth ('depthgrams') and thickness ('thicknessgrams'). The slicing of depthgrams produces tomograms.	[12]

This paper contains the recent results obtained at Tomsk Polytechnic University in the development of some novel approaches to DTT which allow slicing a solid body by analyzing the spatial/temporal evolution of transient surface temperature distributions in one-sided TNDT.

http://dx.doi.org/10.21611/qirt.2010.145
10th International Conference on Quantitative InfraRed Thermography

2. 'Classical' dynamic thermal tomography

This technique proposed in the 1980s is based on the idea to substitute a long image sequence with the pair of images called *maxigram* and *timegram*; a reference point is to be introduced to specify a 'non-defect' behavior of a sample under test [8]. A maxigram represents a specific IR thermogram where each pixel reveals its maximum differential signal ΔT_m in regard to a reference point. In its turn, a timegram is the result of non-linear image treatment which exhibits times τ_m when ΔT_m signals appear. Timegrams can be 'sliced' for thermal tomograms proving to be more user-friendly than trivial IR images.

The efficiency of such 'classical' algorithm can be illustrated on a 10-ply CFRP sample which 'traditionally' contained 25 Teflon inserts by various size located at depths from 0.2 to 1 mm (sample: courtesy W.Świderski), see figure 1. The experimental sequence was obtained by using a computerized IR thermographic system at University Laval, Canada. This sequence seemed to be quite good for the comparison of several data processing algorithms, such as Fourier transform (Pulse Phase Thermography), Principal Component Analysis etc.; these results were reported elsewhere [13].

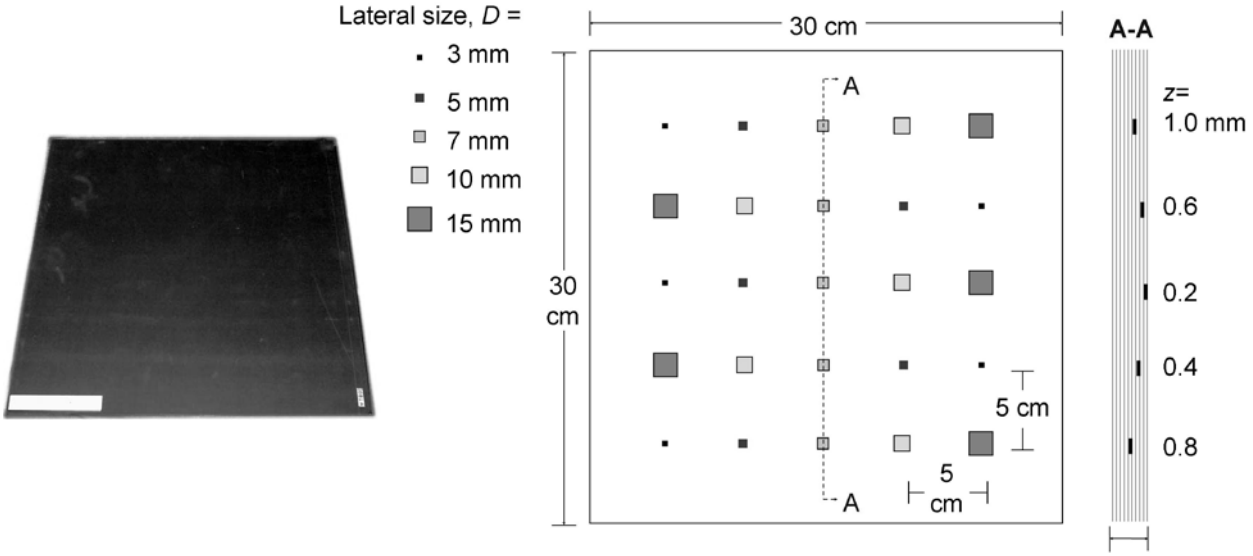

Fig. 1. *CFRP 10-ply 2 mm-thick reference sample (25 Teflon inserts)*

In order to correctly apply the algorithm of thermal tomography, a reference point was chosen close to the defect A shown in figure 2a. The corresponding maxigram and timegram are shown in figure 2b,c. Respectively, in this case the minimal detected defect 10x10 mm was located at the depth of 1 mm.

Thermal tomograms are shown in figures 2d-h. The layers identified have been calibrated by using the CFRP diffusivity value of $0.8 \cdot 10^{-7}$ m^2/s. The obtained tomographic estimates are in a rather good accordance with true values.

The tomograms in figures 2d-f can be regarded 'classical' because they exhibit only real defects located in the selected layers. Oppositely, the tomogram in figure 2h (the deepest layer at the 1 mm depth), along with defect footprints, contains some artifacts caused by defects in other layers (strictly speaking, there is also the artifact in figure 2g). The nature of artifacts was discussed in [12]. In shallow layers, artifacts can be effectively subdued by trivial amplitude filtration, as shown in figures 1d-f. However, in deeper layers, artifacts can be inseparable from real defects because both are of low amplitudes. In some cases, better results can be obtained by using no-reference tomography (see below).

3. No-reference tomography

In DTT, uneven heating makes results strongly dependent on where a reference point is chosen. As a matter of fact, only 'flat' non-defect areas allow thermal tomograms of a good quality across large areas. In order to overcome the necessity of introducing a reference point, the idea of no-reference DTT was proposed. The main concept is to model the temperature evolution in non-defect areas by using, for example, theoretical heat conduction solutions [14] or polynomials [12]. In the latter case, it is assumed that non-defect temperatures can be described by polynomials of a lower order, while subsurface defects cause significant signals in high-order polynomial members.

http://dx.doi.org/10.21611/qirt.2010.145

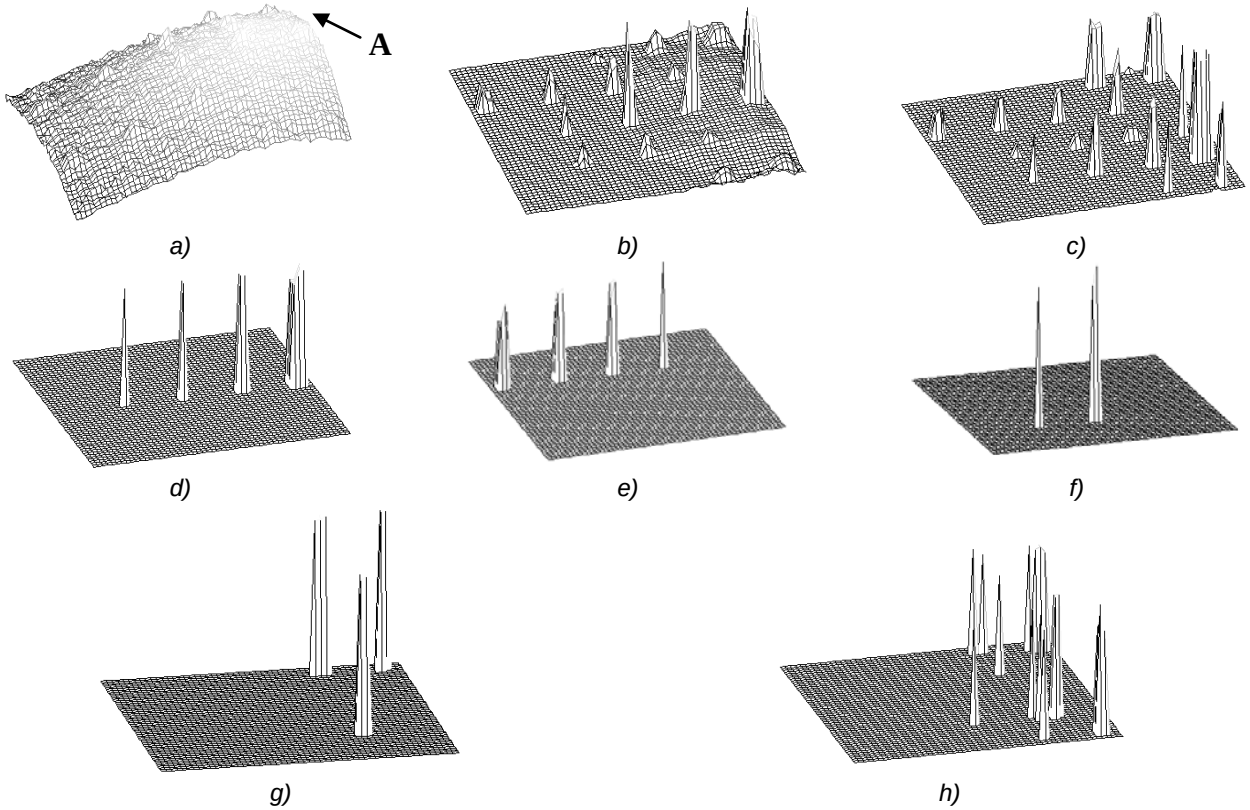

Fig. 2. *Tomographic analysis of a CFRP sample from figure 1:*

a – optimum source image (defect A: SNR=1.0),
b – maxigram,
c – timegram,
d – thermal tomogram, layer 0.24-0.31 mm,
e – thermal tomogram, layer 0.42-0.54 mm,
f – thermal tomogram, layer 0.60-0.66 mm,
g – thermal tomogram, layer 0.67-0.69 mm,
h – thermal tomogram, layer 0.71-0.83 mm

Let us assume that evolutions of both 'defect' and 'non-defect' temperatures can be fitted with polynomials of the m^{th} and n^{th} order respectively, where $m<n$. Differential signals may be defined as $\Delta T_{ij\,f} = T^{(n)}_{ij\,f} - T^{(m)}_{ij\,f}$, where the superscripts specify a degree of a polynomial, and the subscript "*f*" means fitting. Such approach can be applied to each pixel without introducing a reference point; in fact, it is assumed that the m^{th} –order polynomial describes non-defect evolutions, while the n^{th} –order polynomial includes both 'classical' signal behavior and deviations in defect areas. Since differential temporal evolutions involve some local extremums caused by hidden defects, they can be used for producing specific maxigrams and timegrams, thus making possible 'no-reference' tomography.

Preliminary experimental results have been obtained (in collaboration with W.Świderski, WITU, Poland) on a 2 mm-thick CFRP sample, same as in figures 1 and 2. The resulting tomogram of a deeper layer contained no artifacts which accompanied the DTT algorithm (see figure 3).

http://dx.doi.org/10.21611/qirt.2010.145
10th International Conference on Quantitative InfraRed Thermography

a) *b)*

Fig. 3. *Comparison between 'classical' and no-reference DTT algorithms in the inspection of a 2-mm thick CFRP sample:*

a - 'classical' DTT algorithm (multiple artifacts are present at different depths),
b - no-reference DTT algorithm (two defects only at the depth of 0.75-1 mm are seen)

4. Defect characterization

The next approach to thermal tomography is based on the assumption that a relevant defect characterization algorithm may also finish with the discrimination of defects by their depth (along with defect lateral size and thickness), thus resulting in artificial images regarded as thermal tomograms.

There are several data inversion algorithms available in TNDT. For example, the ThermoFit Pro software (Innovation Ltd., Russia) uses the generalized inversion formulas of whose outlook depends on whether maximum running contrasts appear within or after a heat pulse. Also, defect areas are supposed to be always warmer than the background. The only experimental parameters are maximum temperature contrasts and times of their appearance. Other input parameters are material thermal properties, heat pulse duration and thermal conductivity of expected defects. The formulas look as follows:

$$P = A[\alpha(\tau_m - \tau_h)]^B (1 - \lambda_d / \lambda)^C (L / \lambda)^D Fo_h^E Con^F . \quad (1)$$

Here: P is a desired defect parameter (depth l or thermal resistance R_d); α is the thermal diffusivity; τ_m is the time when a maximum running contrast Con appears; τ_h is the heat pulse duration;; λ_d is the thermal conductivity of an expected defect; λ is the thermal conductivity of a material; L is the sample thickness; $Fo_h = \alpha\tau_h / L^2$ is the Fourier number related to the heat pulse duration τ_h; $Con = \Delta T / T$ is the maximum running contrast in a defect area; A, B, C, D, E, F are the coefficients determined by polynomial fitting of numerical results.

Equation (1) was obtained in the assumption that defect lateral size significantly exceeds defect depth (one-dimensional case). In the case of three-dimensional defects, there are some additional members introduced into equation (1). These members involve maximum and minimum defect dimensions determined by an operator directly on the corresponding image (the accuracy of such procedure has been found adequate for practical purposes, namely 5-15%). In such way, heat diffusion around small-size defects can be taken into consideration.

Since, an image of defect depth ('depthgram') is obtained by equation (1), a thermal tomogram can be derived by 'slicing' this equation. The example of such approach is shown in figure 4.

The stability of inversion formulas and a rather short computation time are the advantages of the described approach.

5. Neural networks

Neural networks as the simplest and straightforward step toward artificial intelligence have been considerably explored in NDT with the first works being traced to the 1990s [15]. The corresponding research at Tomsk Polytechnic University started recently to show that this technique can be effectively applied to both defect detection and characterization. In all cases, neural output images are more user-friendly than respective source images due to their binary-like nature. Since neural networks are able to characterize defect depths, they can also produce thermal tomograms. A preliminary result of this approach is shown in figure 5. A simple perceptron implemented on the MatLab platform was trained on sound areas of the sample, see the source image in figure 5a (same image in figure 4a). Then, the obtained binary image exhibited clearly five defects in a CFRP composite located at depths from 1.3 to 2.6 mm (figure 5b).

http://dx.doi.org/10.21611/qirt.2010.145

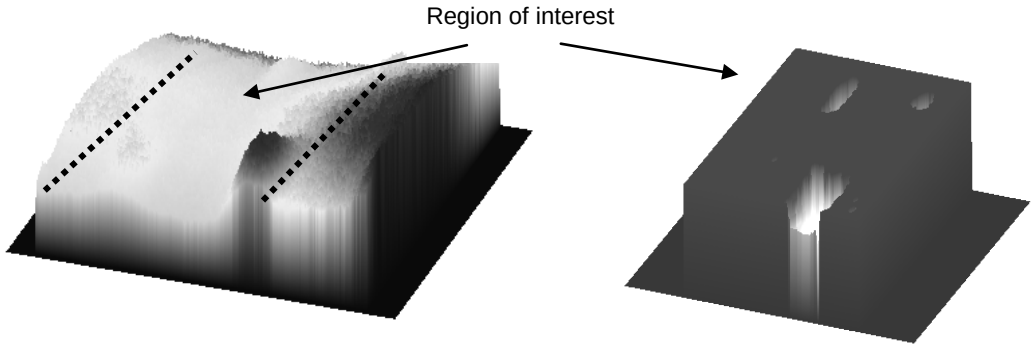

Fig. 4. *Thermal tomogram of the 1.0-1.5 mm layer in a 5 mm-thick CFRP (right) obtained by applying 1D inversion formulas (an optimum source IR image on the left)*

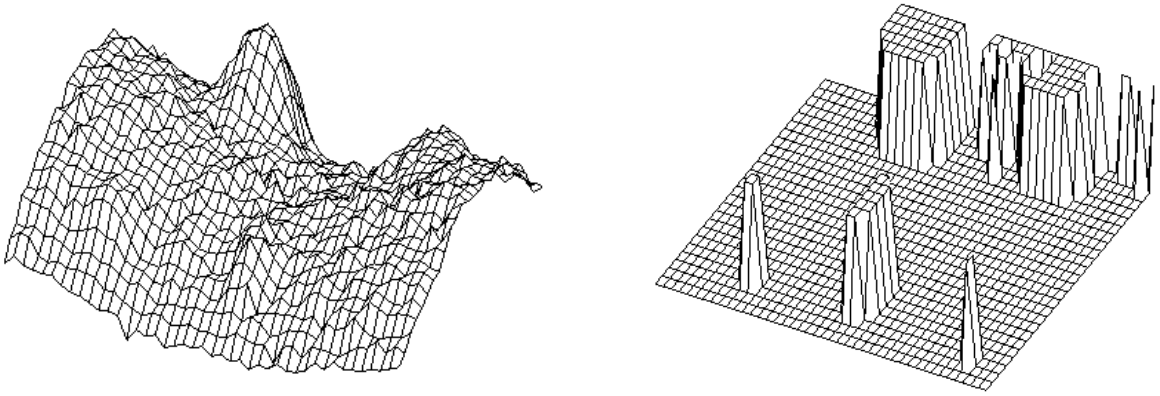

a) *b)*

Fig. 5. *Using a neural network (perceptron) in TNDT of a 5 mm-thick CFRP sample (same as in figure 4):*

a – source IR image,
b – binary map (5 Teflon inserts at depths 1.3 and 2.6 mm)

6. Non-linear fitting

Non-linear fitting is a well-known procedure which is based on the least-square minimization of differences between experimental data and a chosen process model. This technique is particularly good when there is a strong dependence between decision-making parameters, such as differential temperature signals, and parameters to be evaluated, e.g. defect depth. In this study, we have followed the approach proposed in [11]. It seems that a best model for TNDT can be supplied by a solution to the corresponding three-dimensional problem where defect are represented by parallelepipeds of unknown size and depth. However, as the first step to such complicated problem, we have used the known analytical solution to the heating of an adiabatic coating of the thickness l on a semi-infinite substrate:

heating with a Dirac pulse by the energy W:

$$T^F(\tau) = \frac{W}{e_c\sqrt{\pi\tau}}[1 + 2\sum_{n=1}^{\infty}(-\Gamma)^n e^{-\tau^*/\tau}]; \qquad (2)$$

http://dx.doi.org/10.21611/qirt.2010.145
10th International Conference on Quantitative InfraRed Thermography

heating with a square pulse by the power Q:

$$T^F(\tau) = \frac{2Q}{e_c\sqrt{\pi}}[\sqrt{\tau} - \sqrt{\tau - \tau_h} + 2\sqrt{\tau}\sum_{n=1}^{\infty}\Gamma^n \quad F(\tau) - 2\sqrt{\tau - \tau_h}\sum_{n=1}^{\infty}\Gamma^n \quad F(\tau - \tau_h)]; \quad (3)$$

$$F(\tau) = e^{-\tau^*/\tau} - \sqrt{\frac{\pi\tau^*}{\tau}} \; erfc \; (\sqrt{\frac{\tau^*}{\tau}}).$$

step-wise heating:

$$T^F(\tau) = \frac{2Q}{e_c}\sqrt{\frac{\tau}{\pi}}[1 + 2\sum_{n=1}^{\infty}(-\Gamma)^n \cdot\{e^{-\tau^*/\tau} - \sqrt{\frac{\pi\tau^*}{\tau}}\, erfc \; (\sqrt{\frac{\tau^*}{\tau}})\}. \quad (4)$$

.

Here $\tau^* = n^2 l^2 / \alpha_c$ is the specific heat transit time, e_c is the coating effusivity, $\Gamma = (e_s - e_c)/(e_s + e_c)$ is the reflection coefficient; the subscripts "c" and "s" are related to the coating and the substrate respectively,

The presentation of defects in such model is clear from figure 6; for instance, the defect depth is represented by the coating thickness l, while the defect thickness d is evaluated through the reflection coefficient at the coating-substrate boundary.

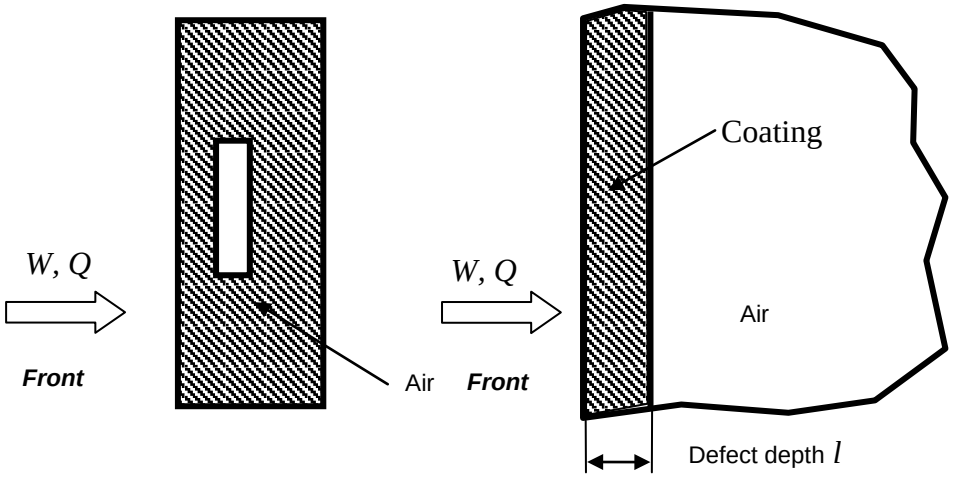

Fig. 6. *Heat conduction model of hidden defects (non-linear fitting algorithm)*

The following model parameters have been identified by using the model above: 1) heating efficiency W / e_c; 2) coating thickness α_c / l^2; 3) reflection coefficient Γ; 4) temporal offset $\Delta\tau_{off}$ (as the additional parameter which accounts for possible temporal de-synchronization of experimental and theoretical data); 5) amplitude offset ΔT_{refl} (as the additional parameter which accounts for possible presence of spurious reflected radiation).

At this research stage, the non-linear fitting algorithm has been verified on the artificial IR image sequence calculated with the ThermoCalc-6L software. The sequence consisted of 250 images and reflected TNDT of a 2 mm-thick CFRP sample which contained 10x10 mm defects at depths from 0.2 to 1.0 mm (modeling the sample in figure 1). The test problem parameters are shown in figure 7 along with a 'quasi-optimal' image (taken at 3.7 s after flash heating). The acquisition frequency was 50 Hz. The corresponding temperature signal evolutions shown in figure 8 are fully 'classical' to reveal maximum differential signals ΔT_m and times of their appearance τ_m.

http://dx.doi.org/10.21611/qirt.2010.145

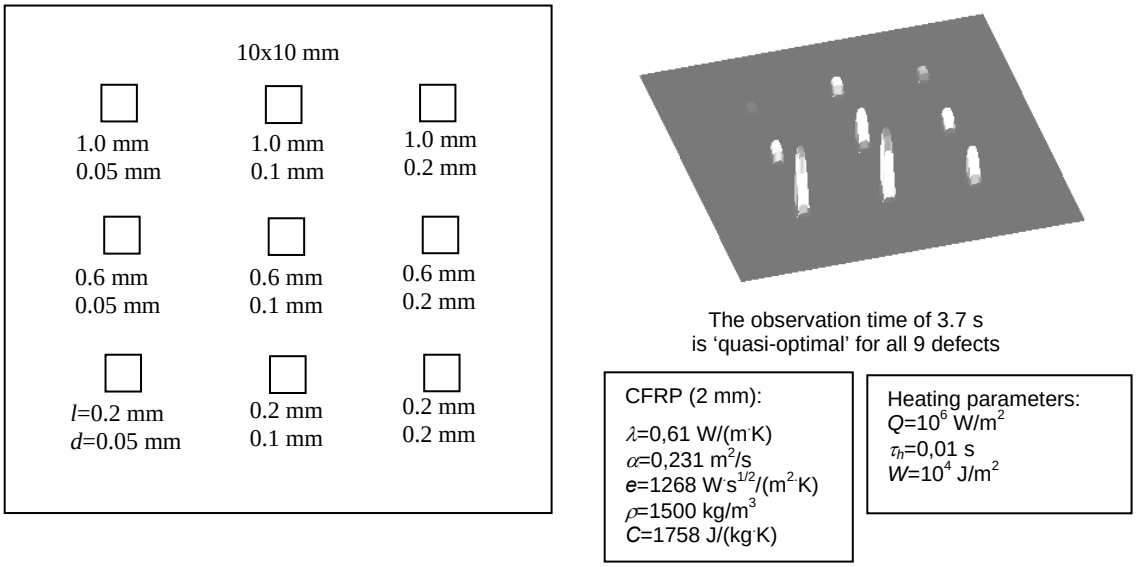

Fig. 7. *Modeling air-filled defects in CFRP*

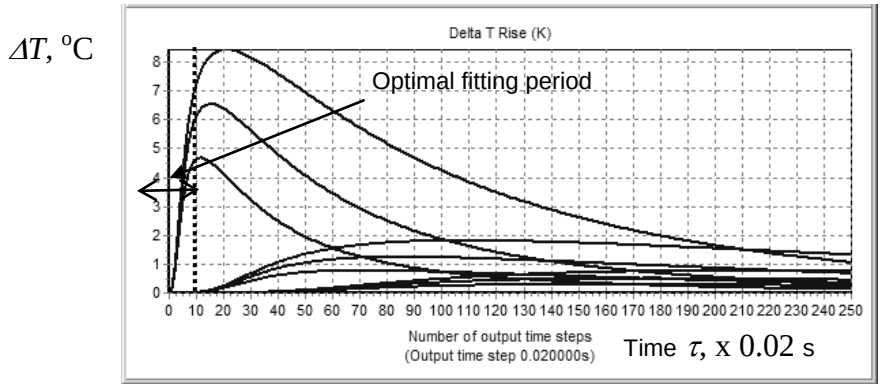

Fig. 8. *Evolution of differential temperature signals in the model from figure 7*

Nonlinear fitting has been applied to the temperature profiles in figure 8. It has been found that the accuracy of fitting mainly depends on a fitting time interval. The best interval seemed to be from the start, i.e. zero, point to the τ_m time, as shown in figure 8. The fitting results by 'defect depth' for 5 defects of 9 total are shown in table 2 to prove reasonable accuracy of defect depth evaluation. It is worth noticing that the efficiency of identifying the reflection coefficient, i.e. the defect thickness, has been much worse that can be explained either by low sensitivity to defect thickness or by inadequacy of the accepted model, or both.

The algorithm described is very time-consuming. The analysis of one pixel requires from several hundreds to several thousands of iterations, thus occupying up to 15 s of processor time (on a 'normal' laptop computer). Therefore, the analysis of a 320x240 frame would require up to 13 days (!).

Table 2. The accuracy of the evaluation of defect depth by using the non-linear fitting algorithm (data in figure 8)

Defect	Evaluated value l, mm	Accuracy, %
l=0.2 mm; *d*=0.1 mm	0.182	9.8
l=0.6 mm; *d*=0.05 mm	0.51	17.6
l=0.6 mm; *d*=0.1 mm	0.52	14.7
l=0.6 mm; *d*=0.2 mm	0.54	11.6
l=1.0 mm; *d*=0.1 mm	0.91	10.3

7. Conclusions

- Unlike the 'classical' dynamic thermal tomography, the no-reference tomography is free of choosing a reference point because it is based on the *a priori* assumption about the 'non-defect' behavior of a sample under test. Non-defect areas are described by low-order polynomial functions while hidden defects cause the appearance of significant higher-order members. This algorithm has been applied to a CFRP sample. The corresponding tomograms contained less artifacts than those obtained 'classically' but the algorithm is cumbersome and requires further analysis.
- The use of a neural network of a simple architecture has produced promising results, at least, if one deals with the enhancement of defect visibility. The synthesis of thermal tomograms requires the use of a network with many outputs that is the goal of further research.
- The known algorithm of non-linear fitting has been applied to a CFRP composite on the base of a simple coating-on-substrate model to evaluate 5 model parameters, including defect depth and thickness. The accuracy of the determination of defect depth has been about 18%, thus principally allowing the synthesis of thermal tomograms. However, this approach cannot be applied to full-frame images because of extremely long computation time.

This research was supported by the grant No. 09-08-13568 from Russian Foundation for Basic Research.

References

[1] Nicolaides L. and Mandelis A., "Experimental and image-inversion optimization aspects of thermal-wave diffraction tomographic Microscopy", Optics Express, Vol. 7, No. 13, p. 519-532, 2000.
[2] Vorontsov S.S., Pikalov V.V., Preobrazhensky N.G. et al., "The algorithm for projections self-matching in IR thermographic tomography", Automation of aerodynamic experiments, Novosibirsk, Institute of theoretical and applied mechanics, Russian Academy of Sciences, p. 63-74, 1985 (in Russian).
[3] Troyitski V.S., "To the theory of contact radiothermometric measurement of inner body temperature", Izvestiya Vuzov, "Radiophysics" series, Vol. 24. No. 9. p. 1054-1058, 1981 (in Russian).
[4] Barrett A., Myers P.S. and Sadowsky N.L., "Detection of breast cancer by microwave radiometer", Radio Sci., Vol. 12, No. 68, p. 167-171, 1977.
[5] Akhmetov V.D. and Fateev N.V., "Infrared tomography of the lifetime and diffusion length of charge carriers in semi-conductive silicon ingots'", Physics and techniques of semiconductors, Vol. 35, No. 1, p 40-47, 2001 (in Russian).
[6] Pasechnik V.I., Anosov A.A., Barabanenkov Yu. N. et al., "Determining in-depth temperature of biological objects by using passive acoustical thermo-tomography", Proc. Nizhny Novgorod acoustical scientific session, NNGU, p. 375-378, 2002 (in Russian).
[7] Busse G. and Renk F., "Stereoscopic depth analysis by thermal wave transmission for NDE", Appl. Phys. Lett., 15 Febr. Vol. 42(4). p. 366-368, 1983.
[8] Vavilov V., Bison P.G., Bressan C., Grinzato E. and Marinetti S., "Some new Ideas in dynamic thermal tomography", Proc. Eurotherm Seminar #27 "Quant. Infrared Thermography-QIRT 92", July 7-9, 1992, Chatenay-Malabry, France, p. 259-255, 1992.
[9] Storozhenko V.A., Melnik S.I. and Orel R.P, "A new algorithm for performing thermal tomography", Methods and equipment for brightness control, No. 4, p. 26-30, 1999 (in Ukranian).
[10] Kush D.V., Rapoport D.A. and Budadin O.N., "Inverse problem of automated thermal NDT", Defectoscopiya (Rus. J. NDT), No. 5, p. 64-68, 1988.
[11] Grinzato E. and Marinetti S., "Materials NDE by non linear filtering applying heat transfer models", Advances in Signal Processing for Non Destructive Evaluation of Materials, Maldague X., ed., NATO ASI Series, Series E: Applied Sciences, Kluwer Academic Publishers, Vol. 262, p. 117-132, 1994.
[12] Vavilov V., "Thermal/Infrared Testing", Nondestructive Testing Handbook, Vol. 5, Spektr Publish., Moscow, 485 p., 2009.
[13] Vavilov V.P., "Thermal (infrared) tomography: terminology, basic procedures and applications to nondestructive testing of composite materials", Defectoscopiya (Rus. J. NDT), No.3, p. 3-15, 2010.
[14] Pilla M., Klen M., Maldague X. and Salerno A., "New absolute contrast for pulsed thermography", Proc. Intern. Quant. Infrared Thermography-QIRT'02 Conf, Sept. 24-27, Dubrovnik, Croatia, p. 53-58, 2002.
[15] Prabhu D.R., Howell P.A, Syed H.I. and Winfree W.P, "Application of artificial neural networks to thermal detection of disbonds", Rev. Progress in Quant. NDE, Thompson D.O. and Chimenti D.E., eds., Plenum Press, New York, Vol.11, p. 1331-1338, 1992.